PAPER

Check for updates

Optimized preparation of gastric acid-response sulfhydryl functionalized chitosan/alginate/tilapia peptide hydrogel and its protective effects on alcohol-induced liver and brain injury

Sitong Lu, Lingyu Zhang, Zhang Hu, [iD]* Songzhi Kong, Zhaoyu Zhang and Guangfa Li

Long-term alcohol intake or drinking large quantities of alcohol at one time can cause organ damage, which in turn can lead to chronic diseases. It is of important clinical and social significance to find effective approaches for the prevention and treatment of alcohol-induced diseases. In this paper, sulfhydryl functionalized chitosan (chitosan-*N*-acetyl-L-cysteine, CS-NAC) and sodium alginate (SA) were used as the matrix materials to contain tilapia peptide (TP), and a gastric acid-response hydrogel (CS-NAC/SA/TP) was prepared. Taking the ethanol adsorption rate as the response index, based on the results of the single factor test, the preparation process of CS-NAC/SA/TP was optimized through the Box–Behnken design. The swelling and antioxidant properties of CS-NAC/SA/TP were tested *in vitro*, and the protective effects on alcohol-induced acute liver injury and chronic brain injury were assessed *in vivo*. Structural characterization showed that CS-NAC/SA/TP was successfully prepared. Under the optimal conditions (SA concentration of 1%, M_{CS-NAC}/M_{CaCO_3} of 1 : 1, $M_{SA}/M_{CS-NAC(CaCO_3)}$ of 15 : 1), the prepared CS-NAC/SA/TP had a porous structure, a swelling ratio of 2350%, an ethanol adsorption rate of 56.23% and strong antioxidant capacities *in vitro*. Animal experiment results demonstrated that CS-NAC/SA/TP effectively reduced liver and brain injuries in mice caused by alcoholism. Summarily, these findings indicate that CS-NAC/SA/TP has potential applications in preventing alcohol-induced liver and brain injuries.

1 Introduction

Alcoholism is a global public health problem, resulting in multiple organ injuries that seriously endanger human life and health.[1] The liver is the critical organ for alcohol metabolism. Excessive alcohol intake will cause an increase in the content of aspartate transaminase (AST) and alanine transaminase (ALT) in the serum, a decrease in the activity of aldehyde dehydrogenase (ALDH) and alcohol dehydrogenase (ADH) in the liver tissue, and hemorrhage, edema, inflammation and necrosis of hepatocytes.[2] As a lipophilic and toxic small molecule, alcohol can pass through the blood–brain barrier and cause brain injury to different degrees,[3] thereby affecting memory and cognitive function and inducing limb tremors, delusions, and hallucinations.[4] Therefore, it is of important clinical and social significance to find effective drugs for the prevention and treatment of alcohol-induced diseases.

Currently, most studies on alcoholic liver and brain injuries mainly focus on abstinence from alcohol, nutritional support, and drug therapy. The goals of drug therapy are to protect the gastric mucosa, control mitochondrial function, enhance antioxidation, regulate cytokines, and resist apoptosis.[5,6] Due to the lack of effective drugs for alcoholic hepatitis and alcohol dependence, it is urgent to develop new therapies.[7,8]

Hydrogels are incredibly hydrophilic three-dimensional network structures with high swelling.[9] Biomacromolecule hydrogels are materials in which polymers are cross-linked by physical, chemical, and other means and play vital roles in various fields.[10,11] Due to their excellent biocompatibility, biodegradability, safety, and specific biological activities, marine natural polysaccharides such as chitin and alginate, have attracted more and more attention in the field of biomedical materials. Chitosan (CS), a semisynthetic polymer obtained through deacetylation of chitin, has the characteristics of excellent biocompatibility, biodegradability, and no toxicity. However, its application is limited by low water solubility and the poor mechanical properties of pure CS hydrogels.[12,13] Sodium alginate (SA) is a biodegradable natural polysaccharide from marine brown algae that can chelate divalent cations (*e.g.*, Ca^{2+}) to form an "egg-carton" conformation with good biocompatibility and strong liquid adsorption capacity. However, the cross-linking density of the three-dimensional network structure of pure alginate is lower than that of the network structure with interpenetrating molecular chains.[14,15]

Department of Applied Chemistry, School of Chemistry and Environmental Science, Guangdong Ocean University, Zhanjiang 524088, China. E-mail: huzhangqyx@126.com

Therefore, hydrogels can be prepared by interpenetrating SA and CS to improve the cross-linking density and enhance hydrogel stability, which can be achieved in acidic conditions once the amine groups of chitosan are protonated. Marine collagen peptides are polypeptides that are separated and extracted from marine natural collagen tissues such as skin, fins, scales, bones, and gallbladder by chemical and enzymatic hydrolysis; they have a wide range of biological activities, such as antioxidation, anti-aging, anti-tumor, antibacterial, angiotensin-converting enzyme inhibition, and wound repair activity.[16] Our previous studies showed that tilapia collagen peptide (TP) from seawater had antioxidant effects and participated in immune regulation, hemostasis, and wound healing.[17] However, active peptides have the disadvantages of instability, short half-life, and low bioavailability in the gastrointestinal tract. It has been reported that it might be a practical approach to overcome these problems by adopting a polymer matrix carrier for drug delivery.[18,19]

The purpose of our work aimed to form a hydrogel *in situ* in the stomach, which can adsorb a large amount of alcohol to prevent its rapid absorption, and simultaneously releases the active peptide, thereby having a protective effect on alcohol-induced liver and brain injury. In this paper, it was first reported that sulfhydryl functionalized chitosan (CS-NAC) was prepared by using CS as the primary raw material to encapsulate nano-CaCO$_3$ to obtain CS-NAC coated calcium carbonate nanoparticles [CS-NAC(CaCO$_3$)]. Under the condition of gastric acid, CS-NAC and SA penetrated each other to encapsulate TP and *in situ* formed the hydrogel (CS-NAC/SA/TP) through non-covalent interactions (including electrostatic interaction between the protonated amino group of chitosan and the carboxyl group of alginate, and the chelation between alginate and Ca^{2+}). Response surface methodology (RSM) was used to optimize the preparation process by taking the ethanol adsorption rate as the response index. Furthermore, animal experiments were conducted to explore the protective effect of hydrogel against alcohol-induced liver and brain injury.

2 Materials and methods

2.1 Materials

Chitosan (molecular weight of 100 kDa, deacetylation degree of more than 90%), sodium alginate (viscosity of 300–500 mpa s), and nano-CaCO$_3$ (70–100 nm) were purchased from Sinopharm Chemical Reagent Co., Ltd. Tilapia collagen peptide was made by our laboratory.[17] ADH and ALDH kits were purchased from Nanjing JianCheng Bioengineering Institute (Nanjing, China) and used according to the manufacturer's instructions.

2.2 Hydrogel preparation

Sulfhydryl functionalized chitosan (chitosan-*N*-acetyl-L-cysteine, CS-NAC) preparation was performed by using the ethyl-3-(3-dimethyl aminopropyl)carbodiimide (EDC)/1-hydroxybenzotriazole (HOBt) method.[20] Briefly, 0.50 g of CS was dispersed in 50 mL of deionized water, HOBt (0.35 g, 2.58 mmol), *N*-acetyl-L-cysteine (NAC, 0.84 g, 5.16 mmol), and EDC·HCl (0.20 g, 10.32 mmol) were added under

magnetic stirring, the pH of the reaction mixture was adjusted to 5.0, and the mixture was stirred at room temperature for 3 h. The reaction mixture was dialyzed for 3 days, freeze-dried, and stored at 4 °C. Through high-speed mechanical stirring (8000 rpm) and ultrasonic treatment, nano-CaCO$_3$ was dispersed in ethanol–water (1 : 2, v/v) solution. CS-NAC(CaCO$_3$) was obtained by dropwise adding homogeneously dispersed nano-CaCO$_3$ solution to CS-NAC solution at low temperature with continued magnetic stirring for 1 h. Next, the solutions were centrifuged at 4 °C at 15 000 rpm for 20 min and freeze-dried. Under ultrasound assistance, an appropriate amount of CS-NAC(CaCO$_3$) was dispersed in SA solution with a specific concentration to obtain the suspension solution that produced CS-NAC/SA when the simulated gastric fluid (SGF, pH 1.2) was added. Similarly, before CS-NAC(CaCO$_3$) was dispersed in the SA solution, TP was added to the SA solution, followed by the same process as the preparation of CS-NAC/SA to obtain CS-NAC/SA/TP hydrogel.

2.3 Determination of ethanol adsorption rate

2 mL of hydrogel precursor solution was mixed with 2 mL of SGF in a centrifuge tube, and the mixture was incubated in a water bath at 37 °C for 30 min. Next, 30% ethanol (v/v) was added, the tube was shaken well, and placed in the water bath for another 30 min before centrifuging at 4500 rpm for 15 min. The solution was collected and measured, and 1 mL of the mixture was taken for determination. Ethanol content was determined by gas chromatography (Agilent GC 8890, Santa Clara, CA, US) with a flame ionization detector. Nitrogen was used as the carrier gas at a flow rate of 1.0 mL min^{-1}. The oven temperature was programmed as follows: maintained at 45 °C for 7 min, rose to 140 °C at a rate of 5 °C min^{-1}, and then rose to 240 °C at a rate of 8 °C min^{-1}. The injector and the detector were at 250 °C. Each sample was measured in triplicate, and the ethanol adsorption rate of hydrogel was calculated as follows:

$$\text{ethanol adsorption rate } (\%) = \frac{m_0 - m_t}{m_0} \times 100 \qquad (1)$$

where m_t and m_0 were the mass of measured and added ethanol, respectively.

2.4 Single-factor tests and RSM optimization

The factors that affect hydrogel ethanol adsorption were as follows: SA concentration (%, 0.5, 1.0, 1.5, 2.0, 2.5), $M_{\text{CS-NAC}}/M_{\text{CaCO}_3}$ (g g^{-1}, 4 : 1, 2 : 1, 1 : 1, 1 : 2, 1 : 4), and $M_{\text{SA}}/M_{\text{CS-NAC (CaCO}_3)}$ (g g^{-1}, 5 : 1, 10 : 1, 15 : 1, 20 : 1, 25 : 1). Based on the single-factor test results, the hydrogel ethanol adsorption rate was taken as the response value. A Box–Behnken design was used to select the three factors and three levels, and RSM was used for optimization.

2.5 Characterizations

The Fourier Transform Infrared (FT-IR) spectra of the samples were measured by infrared spectroscopy (Spectrum100, PerkinElmer, Waltham, MA, US). The wavenumber ranged from 4000 to 400 cm^{-1}, and the resolution was 4 cm^{-1}.

The size and zeta potential of $CaCO_3$ and $CS\text{-}NAC(CaCO_3)$ were analyzed by dynamic light scattering through a laser particle size analyzer (Zetasizernano ZS90, Malvern, UK).

The morphology of the hydrogel was observed by scanning electron microscopy (SEM, S-4800, Japan) using the freeze-dried sample at the acceleration voltage of 20 kV. Before observation, the sample was treated by coating with an ultra-thin gold under a high vacuum.

2.6 Determination of swelling ratio

The swelling property was determined by measuring the amount of water absorbed by hydrogel in SGF. Freeze-dried hydrogel with a known weight was immersed in 10 mL of SGF and incubated for 2.5 h. The hydrogel was removed every 30 min, surface water was wiped off with a piece of filter paper, and the weight was measured. Experiments were performed in triplicate, and the average value was taken. The swelling ratio was calculated as:

$$\text{swelling ratio } (\%) = \frac{m_t - m_0}{m_0} \times 100 \tag{2}$$

where m_0 was for the mass of freeze-dried hydrogel and m_t represented the hydrogel mass after water adsorption.

2.7 Anti-oxidation properties

2.7.1 Determination of 1,1-diphenyl-2-picrylhydrazyl free radical (DPPH·) scavenging activity. Samples were mixed with DPPH alcohol solution. After 30 min at room temperature from light, the absorbance was measured at 517 nm. Distilled water was used as a blank control. The scavenging activity of DPPH· was calculated as equation (eqn (3)):

$$\text{scavenging activity } (\%) = \frac{A_{x_0} - A_x}{A_{x_0}} \times 100 \tag{3}$$

where A_x and A_{x_0} are the absorbances of the sample and blank control, respectively.

2.7.2 Determination of peroxide-free radical ($O_2^{·-}$) scavenging activity. 0.5 mL of tris(hydroxymethyl)aminomethane hydrochloride (Tris–HCl, pH 8.2) was mixed with 0.1 mL of pyrogallol solution (3 mmol L^{-1}) in a test tube. The mixture was incubated at room temperature for 15 min. Next, the sample was added and kept for 5 min at room temperature. And the absorbance of the mixture was measured at 320 nm. Distilled water was used as blank control. The scavenging activity of $O_2^{·-}$ was calculated according to eqn (3).

2.7.3 Determination of hydroxyl radical (·OH) scavenging activity. 1 mL of H_2O_2 solution (8.8 mmol L^{-1}), 1 mL of $FeSO_4$ solution (9 mmol L^{-1}), and 12 mL of sample solution were added to the same colorimetric tube, then 1 mL of alcohol solution containing salicylic acid (9 mmol L^{-1}) was added. The tube was shaken well, placed in a 37 °C water bath for 30 min, and the absorbance was measured at 510 nm. Distilled water was used as blank control. The scavenging activity of ·OH was calculated according to eqn (3).

2.8 Protective effect of hydrogel on acute alcoholic liver injury in mice

2.8.1 Grouping of mice. Male Kunming mice (20–25 g in weight, 28–35 days old) of specific pathogen-free grade were purchased from Guangdong Laboratory Animal Science Center (License no.: SYXK (Guangdong): 2014–0053). Mice were kept in a room with temperature (22–23 °C) and humidity (46–63%). After adaptive feeding for 1 week, the mice were randomly divided into six groups: normal, model, KingDrink control (positive), TP, CS-NAC/SA, and CS-NAC/SA/TP groups.

2.8.2 Modeling of acute alcoholic liver injury in mice. Sixteen mice in each group were given a corresponding volume of tested samples by gavage (10 mL per kg per body weight (BW)) once a day for 7 consecutive days. The normal and model groups were given corresponding volumes of distilled water. After 6 days, the mice were fed with tested samples and fasted for 24 h with access to water. After 60 min, five groups of mice were given 56° KingDrink, while the normal group received an equal volume of distilled water (13 mL per kg per BW). Samples were collected after 60 min.

2.8.3 Liver coefficient. Each liver was removed and weighed, and the liver index was calculated according to the following formula:

$$\text{liver index } (\%) = \frac{m_{\text{liver}}}{m_{\text{body}}} \times 100 \tag{4}$$

2.8.4 Serum biochemical analysis. Blood was collected from the posterior orbital venous plexus and centrifuged at 4 °C and 3500 rpm for 5 min to collect serum. The contents of ALT and AST in serum were determined by a fully automatic biochemical analyzer (HITACHI 7020, Tokyo, Japan).

2.8.5 Determination of ALD and ALDH activities in liver tissue. A 10% liver homogenate preparation was obtained by mixing 1.00 g liver tissue with 9 mL ice normal saline on ice by cryomill (JXFSTPRP-CL, Shanghai, China) and centrifuging at 4000 rpm min^{-1} for 10 min. Liver tissue activities of ADH and ALDH were determined according to the instructions of ADH and ALDH kits.

2.8.6 Hematoxylin and eosin (H&E) staining analysis of liver tissue. H&E staining was carried out for liver histopathological sections. The isolated left lobe was fixed in 4% paraformaldehyde, gradually dehydrated with gradient alcohol, made transparent in xylene, embedded in paraffin, sectioned, stained, and observed under an optical microscope.

2.9 Effect of hydrogel on chronic alcoholic brain injury in mice

2.9.1 Modeling of chronic alcoholic brain injury in mice. Modeling and treatment of chronic alcoholic brain injury in mice were performed as follows: Fourteen mice in four groups were given 56° KingDrink, while the normal and model groups were provided with equivalent volumes of distilled water. The mice were weighed weekly to adjust the dosage. In the first week, the amount of alcohol consumed was 2 mL per kg per BW. The amount of alcohol consumed was appropriately increased

Paper

RSC Advances

every week to cause persistent alcohol injury. Continuous gavage lasted for 8 weeks. The model group was given distilled water according to 10 mL per kg per BW after drinking for 1 h.

2.9.2 Morris water maze experiment. The ability of animals to learn and remember spatial position and direction was tested by observing the water maze's hidden platforms. Morris water
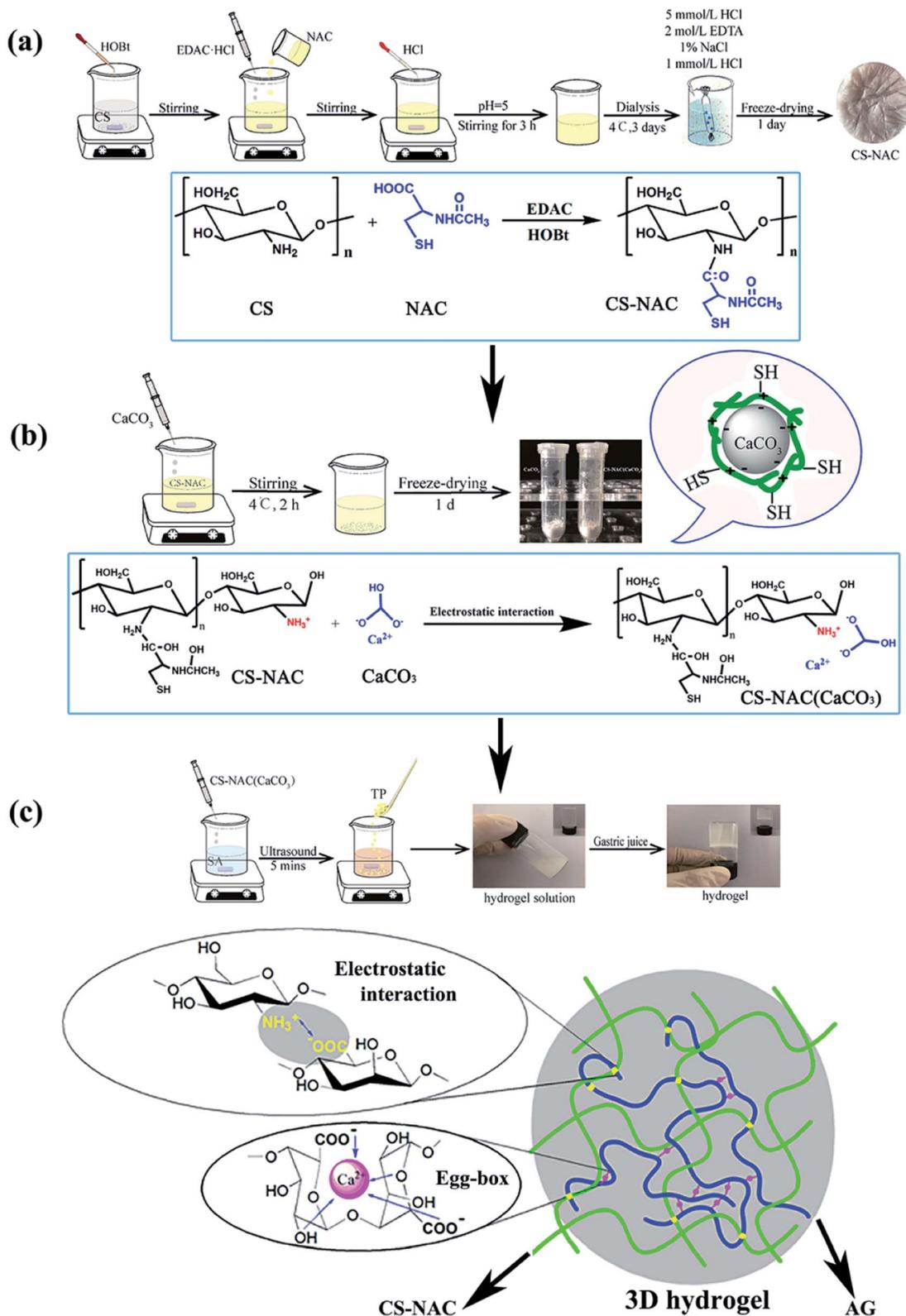

Fig. 1 Preparation of hydrogels: (a) synthesis of CS-NAC; (b) coating CaCO₃ with CS-NAC; (c) formation of hydrogels.

maze testing was carried out 8 weeks after alcohol injury. Mice swam in a black round pool with a diameter of 120 cm and a height of 40 cm. The pool was filled with water and contained a movable platform with a diameter of 8 cm. The experiment lasted for 5 days, 4 times a day, and the mouse was placed into the pool from four different starting points. The video recorded the time when the mice found the platform (escape latency). On the 6th day, the original platform was removed, and the mice were put into the water at a random entry point. The time the mice spent where the platform was located, the number of crossings, and the path was recorded.

2.9.3 Brain index. After the Morris water maze experiment, mice were fasted for 24 h and killed by dislocation. The brain tissue was taken out and weighed.

$$\text{brain index } (\%) = \frac{m_{brain}}{m_{body}} \times 100 \qquad (5)$$

2.10 Statistical analysis

The data were processed with IBM SPSS Statistics 26 software (Armonk, NY, USA) and analyzed by independent sample t-tests to demonstrate differences between groups. p values <0.05 and <0.01 were considered to be statistically significant and highly significant, respectively.

3 Results and discussion

3.1 Preparation of gastric acid-response hydrogels

The preparation process of CS-NAC/SA/TP hydrogel included three steps: Synthesis of CS-NAC, coating $CaCO_3$ with CS-NAC, and formation of hydrogel CS-NAC/SA/TP (Fig. 1). To improve the physicochemical properties of CS, especially the mucoadhesion of the hydrogel to prolong its residence time in the stomach, sulfhydryl functionalized chitosan was synthesized. As shown in Fig. 1(a), the primary amino group on CS reacted with the carboxyl group of NAC to obtain CS-NAC *via* amide bond formation mediated by EDC. Through adhesion and electrostatic interaction, CS-NAC could encapsulate nano-$CaCO_3$ to yield CS-NAC ($CaCO_3$) shown in Fig. 1(b). Subsequently, a polyelectrolyte complexing hydrogel precursor was prepared by uniformly dispersing CS-NAC ($CaCO_3$) into an alginate solution.[21] Once gastric acid was injected into the precursor solution, CS-NAC and SA penetrated each other and *in situ* formed a three-dimensional hydrogel (CS-NAC/SA). During CS-NAC dissolution, gastric acid gradually contacted and decomposed $CaCO_3$ to release Ca^{2+}, a classic egg-box cross-linking of calcium alginate was produced to form uniform hydrogel which further enhanced the mechanical strength of the hydrogel (Fig. 1(c)).[22] When TP was added to the precursor solution, the gastric acid-response hydrogel of CS-NAC/SA/TP was obtained.

3.2 Single-factor test analysis

3.2.1 Effect of SA concentration on the alcohol adsorption rate of hydrogel. Fig. 2(a) showed the effect of SA concentration
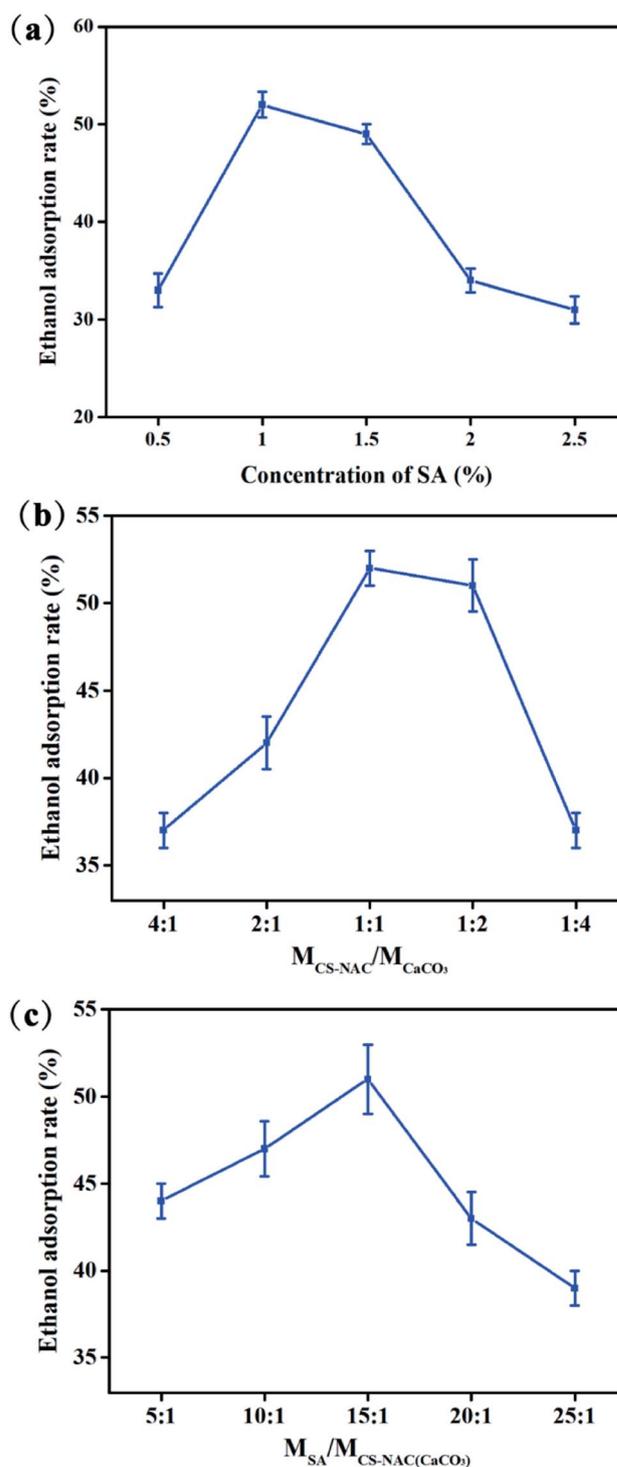

Fig. 2 Single-factor test analysis: (a) effect of SA concentration on ethanol adsorption rate; (b) effect of M_{CS-NAC}/M_{CaCO_3} on the ethanol adsorption rate; (c) effect of $M_{SA}/M_{CS-NAC\ (CaCO_3)}$ on the ethanol adsorption rate.

on the alcohol adsorption rate of the hydrogel. The ethanol adsorption rate of hydrogel increased first and then decreased with SA concentration, reaching a maximum value of 52.03% at an SA concentration of 1%. If the concentration of SA is too low,

Table 1 RSM experimental results

Runs	A SA concentration (%)	B $M_{\text{CS-NAC}}/M_{\text{CaCO}_3}$	C $M_{\text{SA}}/M_{\text{CS-NAC (CaCO}_3)}$	Ethanol adsorption rate (%)
1	0.5	1 : 2	15 : 1	34.22 ± 1.02
2	1.5	1 : 2	15 : 1	29.54 ± 0.98
3	0.5	1 : 1	15 : 1	36.32 ± 1.31
4	1.5	2 : 1	15 : 1	42.45 ± 2.56
5	0.5	1 : 1	10 : 1	32.56 ± 1.65
6	1.5	1 : 1	10 : 1	28.31 ± 1.02
7	0.5	1 : 1	20 : 1	30.43 ± 1.67
8	1.5	1 : 1	20 : 1	34.42 ± 1.54
9	1.0	1 : 2	10 : 1	49.45 ± 3.65
10	1.0	2 : 1	10 : 1	40.52 ± 2.34
11	1.0	1 : 2	20 : 1	46.61 ± 3.31
12	1.0	2 : 1	20 : 1	35.25 ± 2.02
13	1.0	1 : 1	15 : 1	59.35 ± 3.03
14	1.0	1 : 1	15 : 1	52.43 ± 3.89
15	1.0	1 : 1	15 : 1	54.19 ± 3.02
16	1.0	1 : 1	15 : 1	56.20 ± 3.23
17	1.0	1 : 1	15 : 1	53.43 ± 2.42

the hydrogel will not be formed. Conversely, if the concentration is too high, the hydrogel will have problems such as hardness, small pores, concrete blocks, and others that will result in difficult infiltration, thus reducing the adsorption rate of ethanol.

3.2.2 Effect of $M_{\text{CS-NAC}}/M_{\text{CaCO}_3}$ on the ethanol adsorption rate of hydrogel. Due to the pH sensitivity of $CaCO_3$, the coating layer of CS-NAC/$CaCO_3$ will affect the release of Ca^{2+}, which will significantly affect the hydrogel structure.[23] Fig. 2(b) showed the effect of $M_{\text{CS-NAC}}/M_{\text{CaCO}_3}$ on the ethanol adsorption rate of the hydrogel. It firstly increased and reached a maximum value of 52.12% at a 1 : 1 ratio, and then began to decrease when $CaCO_3$ exceeded CS-NAC, indicating that the appropriate coating layer of CS-NAC/$CaCO_3$ was conducive to the formation of hydrogel with high ethanol adsorption rate. It can be reasonably explained that when insufficient CS-NAC was coated on the $CaCO_3$ surface, $CaCO_3$ was rapidly decomposed by H^+ in gastric acid to release a large amount of Ca^{2+} and form a hydrogel with dense structure, resulting in low ethanol adsorption rates.

3.2.3 Effect of $M_{\text{SA}}/M_{\text{CS-NAC(CaCO}_3)}$ on the ethanol adsorption rate of hydrogel. CS-NAC/SA/TP was a hydrogel that formed a stable spatial structure by multiple interactions, especially electrostatic interaction.[24] Fig. 2(c) showed the effect of $M_{\text{SA}}/M_{\text{CS-NAC(CaCO}_3)}$ on the ethanol adsorption rate of the hydrogel. As $M_{\text{SA}}/M_{\text{CS-NAC(CaCO}_3)}$ increased, the ethanol adsorption rate of the hydrogel first increased and then decreased, reaching the maximum value of 51.34% at $M_{\text{SA}}/M_{\text{CS-NAC(CaCO}_3)}$ of 15 : 1. This may be due to forming a good penetration structure between SA and CS-NAC, which was beneficial to ethanol adsorption.

Table 2 Analysis of variance for regression

Source	Sum of squares	Degrees of freedom	Mean square	F value	p-Value (prob. > F)
Model	1656.18	9	184.02	15.45	0.0008
A	504.75	1	504.75	42.39	0.0003
B	0.92	1	0.92	0.077	0.7895
C	69.75	1	69.75	5.86	0.0461
AB	145.53	1	145.53	12.22	0.0100
AC	16.00	1	16.00	1.34	0.2844
BC	3.79	1	3.79	0.32	0.5903
A^2	1233.55	1	1233.55	103.60	<0.0001
B^2	123.41	1	123.41	10.36	0.0147
C^2	99.28	1	99.28	8.34	0.0234
Residual	83.35	7	11.91	—	—
Lack of fit	52.55	3	17.52	2.27	0.2219
Pure error	30.80	4	7.70	—	—
Cor total	1739.53	16	—	—	—

$R^2 = 0.9521$ $R_{\text{adj}}^2 = 0.8905$

3.3 RSM optimization

Based on the results of single-factor tests, a Box–Behnken experimental design was adopted by taking the ethanol adsorption rate of CS-NAC/SA/TP as the response value. Table 1 showed 17 test combinations with three factors and three levels.

By using the Box–Behnken analysis method in the software Design-Expert 8.05, the quadratic polynomial regression equation was obtained as follows:

$$Y = -48.23 + 113.35A + 3.48B + 5.76C + 25.30AB + 0.80AC - 0.25BC - 73.83A^2 - 11.97B^2 - 0.21C^2.$$

As shown in Table 2, the regression model has high significance ($p < 0.01$). The determination coefficient (R^2) was 0.9521, demonstrating that the regression equation had an excellent fitting degree. The lack of fit was not significant ($p = 0.2219$), which indicated that the model fitting was not distorted and the experimental error was small. According to the F value, the influence order of three factors on the ethanol adsorption rate of CS-NAC/SA/TP was as follows: SA concentration $> M_{CS-NAC}/M_{CaCO_3} > M_{SA}/M_{CS-NAC(CaCO_3)}$.

Combined with the interaction response of influencing factors (Fig. 3) and actual operation, the optimal process conditions for achieving a maximum ethanol adsorption rate (55.19%) were as follows: SA concentration of 1%, M_{CS-NAC}/M_{CaCO_3} of 1 : 1, and $M_{SA}/M_{CS-NAC(CaCO_3)}$ of 15 : 1. The verified results showed that the ethanol adsorption rate of the hydrogel prepared was 56.23%, and the relative error was 2.8%, confirming that the optimization model had high credibility.

3.4 Structure analysis

To elucidate that *N*-acetyl-L-cysteine (NAC) has been grafted onto chitosan, the proton nuclear magnetic resonance (^{1}H NMR) spectra of CS and CS-NAC were performed. As shown in Fig. 4(a), the 1H NMR spectrum of CS showed that a peak at 1.80 ppm corresponded to –CH$_3$ of acetylated residues. The peaks at 3.16 ppm (H2), 3.55–3.95 ppm (H3–H6), and 4.70 ppm (H1) were observed, corresponding to the protons of chitosan pyran rings, which were consistent with the previous reports.[25] Compared with the CS spectrum, it could be found from the ^{1}H NMR spectrum of CS-NAC that the peak at 1.87 ppm was significantly enhanced, corresponding to the –CH$_3$ present in both CS and CS-NAC entities. A new resonance at 2.80 ppm appeared, corresponding to the –CH$_2$S– of NAC. According to the proton integral area ratio of –CH$_2$S– to H2, it can be calculated the substitution degree of CS-NAC was about 9%.

CS-NAC is a kind of polycationic electrolyte that can interact with the negatively charged nano-CaCO$_3$ on the surface to form a coating layer by electrostatic attraction.[26] To confirm the formation of the coating layer and the occurrence of electrostatic interaction, we conducted the measurement of the particle size and zeta potential by using a Z-analyzer, and the results were given in Fig. 4(b). The average diameter and zeta potential of CaCO$_3$ were 158.7 ± 2.1 nm and −3.50 ± 0.52 mV, respectively. By coating CaCO$_3$ with 1 g mL^{-1} of CS-NAC

solution, the average diameter and zeta potential of CS-NAC(CaCO$_3$) were 203.0 ± 6.8 nm and −3.09 ± 0.16 mV, respectively. Compared with CaCO$_3$, both the average diameter and zeta potential of CS-NAC(CaCO$_3$) were significantly increased ($p < 0.01$), which further suggested that a layer of CS-NAC was formed on the surface of CaCO$_3$. Since CS-NAC was a polycationic polymer containing protonated amino groups,[27] the positively charged CS-NAC coated onto negatively charged
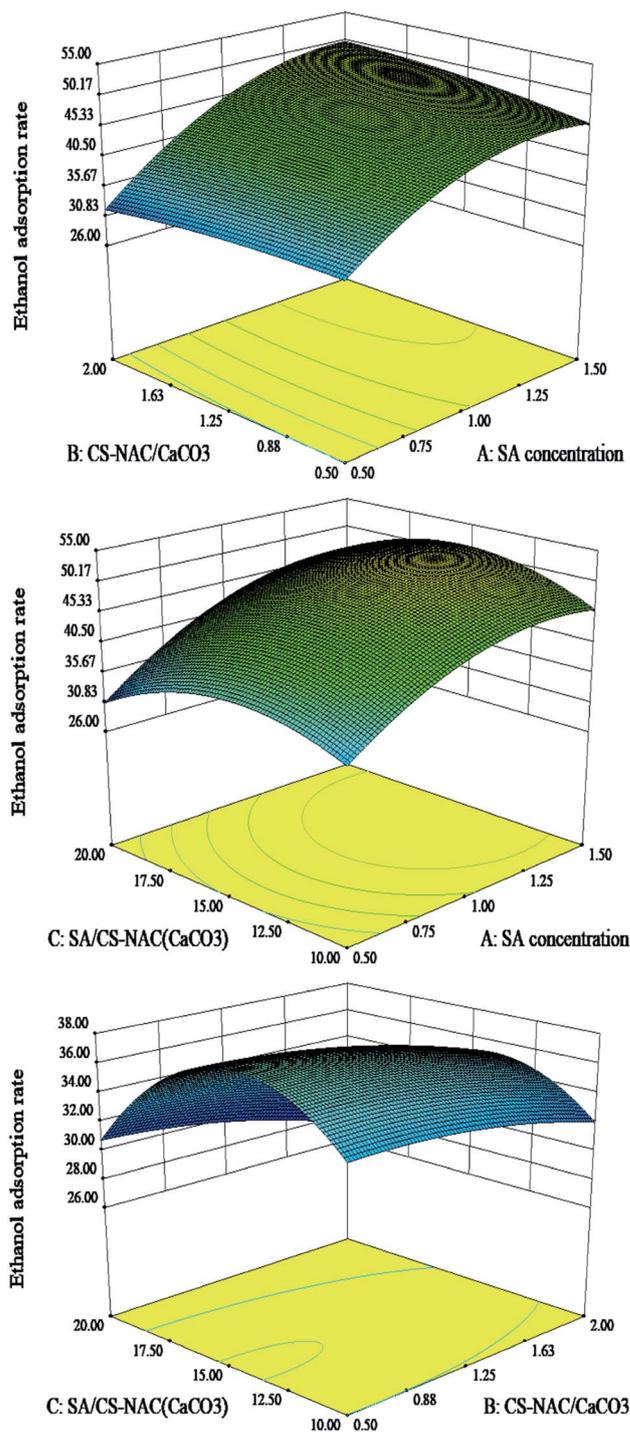

Fig. 3 Response surface of the interaction of experimental factors.

$CaCO_3$ particles through electrostatic interaction, thereby forming a thin layer at the interface. Therefore, the result of electrostatic interaction can reasonably explain the increase in particle size and zeta potential of CS-NAC ($CaCO_3$).

Fig. 4(c) showed the FT-IR spectra of SA, CS-NAC, CS-NAC/SA, TP, and CS-NAC/SA/TP. In the spectrum of SA, the absorption peaks at 1594 and 1405 cm^{-1} were attributed to the asymmetric and symmetric stretching vibrations of the carboxylate group (–COO–), respectively. By comparing the spectrum of CS-NAC/SA with SA and CS-NAC, a broader and stronger stretching vibration of O–H at 3500–3200 cm^{-1} was observed, indicating the enhanced hydrogen bonds.[28] The absorption peaks of CS-NAC at 1649 cm^{-1} and 1591 cm^{-1} disappeared in the hydrogel due to the protonation of –NH$_2$ into –NH$_3^+$.[29] The characteristic absorption peaks of –COO– shifted to 1597 and 1407 cm^{-1}, respectively, suggesting that the physical cross-linking have occurred, including the ionic cross-linking of alginate with Ca^{2+} and the electrostatic interaction between COO– and NH$_3^+$. From the infrared spectrum of TP, the characteristic amide A and B bands of TP were observed at 3300 and
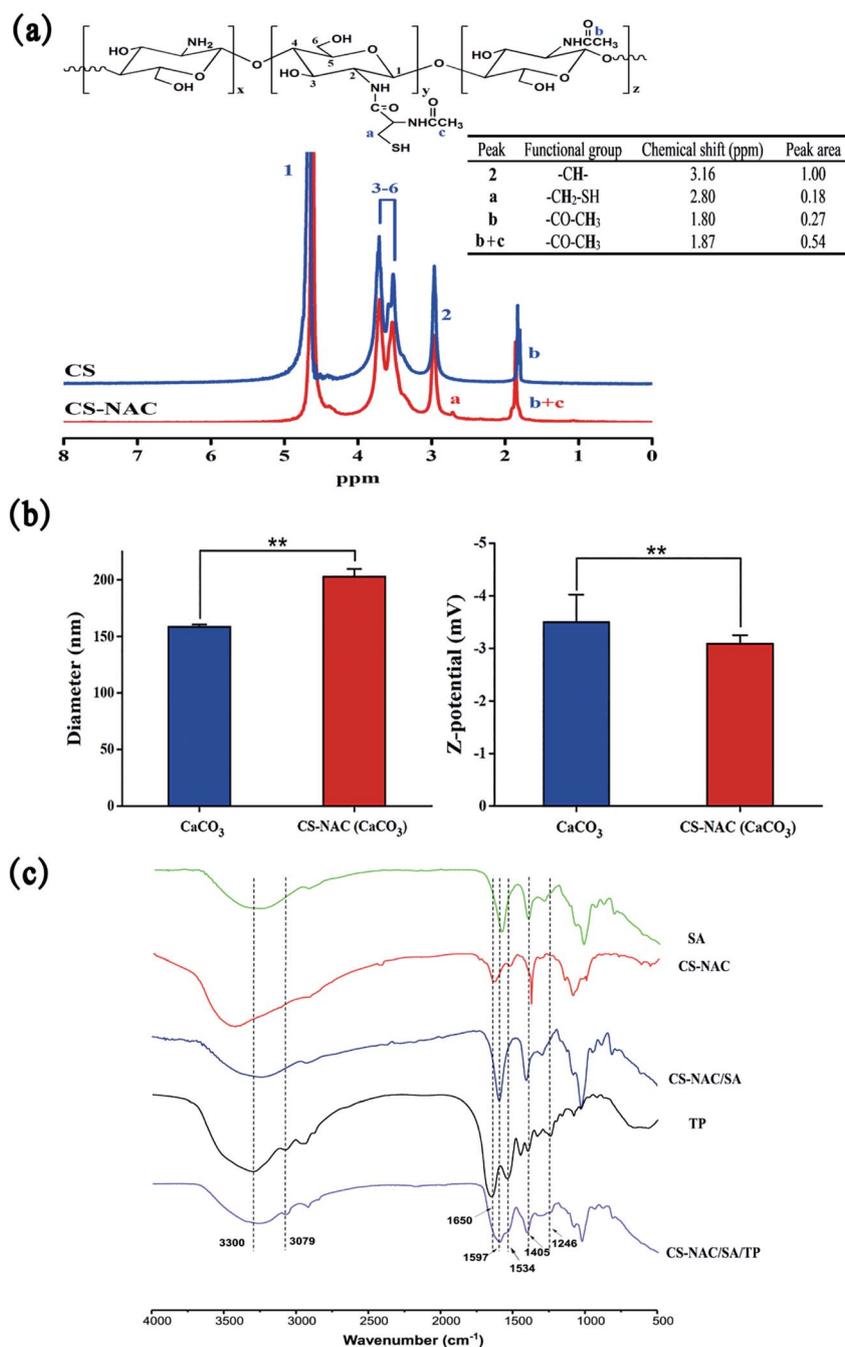
Fig. 4 Structure characterizations: (a) ^{1}H NMR spectra of CS and CS-NAC; (b) diameter and zeta potential of nanoparticles; (c) FT-IR spectra of samples.

3079 cm^{-1}, respectively. The characteristic absorption peaks at 1650, 1534, and 1246 cm^{-1} were assigned to amide I, II, and III bands of peptides, respectively.[30] Compared with CS-NAC/SA, CS-NAC/SA/TP exhibited additionally the prominent characteristic absorption peaks of TP at 3300 and 3079 cm^{-1}, which indicated that TP had been successfully encapsulated into the hydrogel.

3.5 Morphology analysis and swelling property

The surface morphologies of the lyophilized hydrogel was observed by scanning electron microscopy (SEM), and the results were shown in Fig. 5(a). The surface of the hydrogel had an irregular porous structure, and the pore diameter was approximately 30–100 μm. The excellent pore structure of CS-NAC/SA/TP was conducive to the adsorption of ethanol and the release of TP.
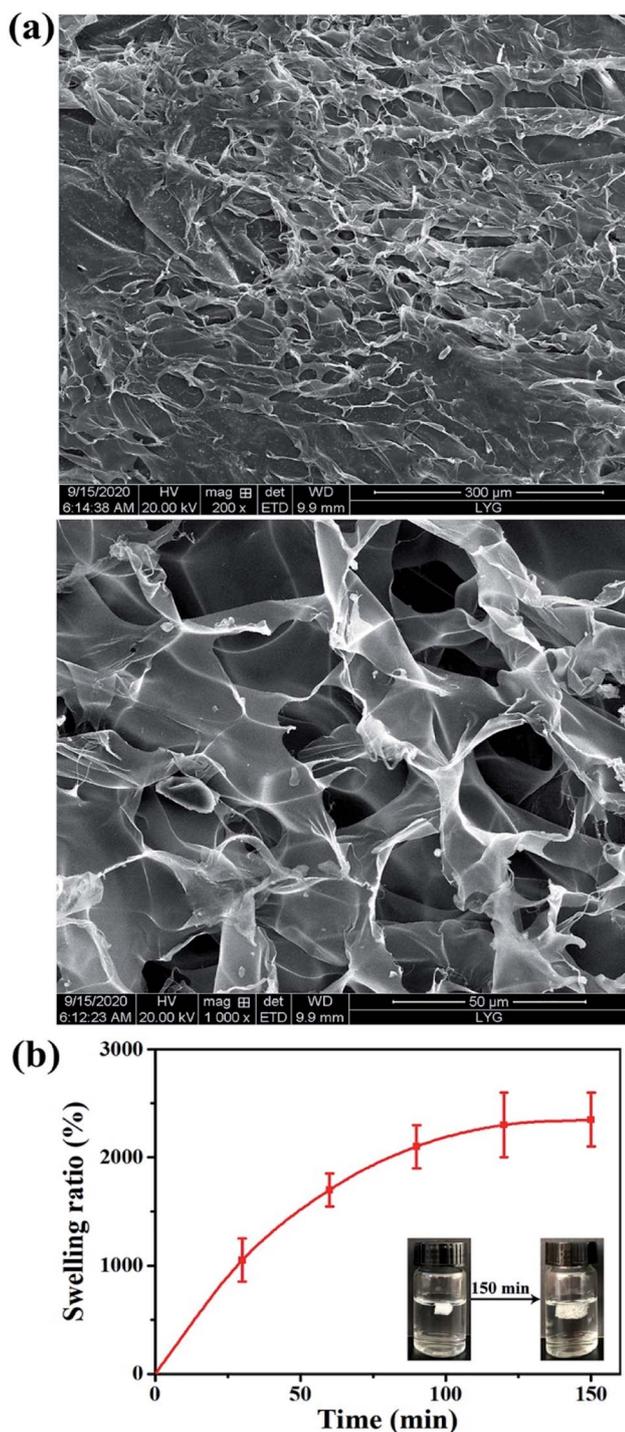
Fig. 5 (a) SEM micrographs, and (b) swelling ratio of CS-NAC/SA/TP.
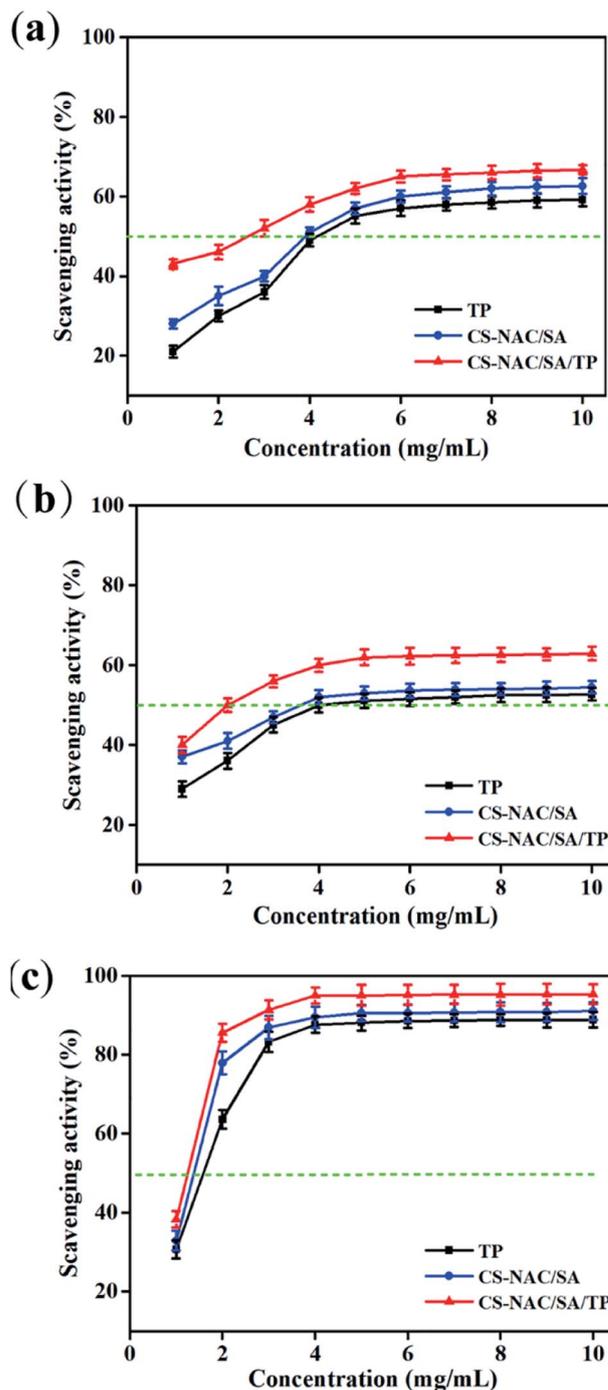
Fig. 6 Free radical scavenging activity of samples: (a) $^{\bullet}$DPPH; (b) $O_2^{\bullet-}$; and (c) $^{\bullet}$OH.

The swelling behavior of CS-NAC/SA/TP in simulated gastric fluid (SGF, pH 1.2) was shown in Fig. 5(b). With the increasing of time, the swelling ratio of CS-NAC/SA/TP gradually increased and rapidly absorbed water and expanded before 90 min, until the swelling ratio reached 2350% after 150 min. The hydrogel maintained its structural integrity after water adsorption. This suggested that CS-NAC/SA/TP could swell and retain a large amount of ethanol due to the three-dimensional network structure. Since the hydrophilicity of sulfhydryl groups is lower than that of hydroxyl and amino groups, sulfhydryl functionalization of chitosan will reduce the swelling of the hydrogel. However, sulfhydryl groups can cross-link polymer chains *via* disulfide bridges. Therefore, sulfhydryl functionalization of chitosan produced a strong network which was desired for wound healing applications.[31]

3.6 Antioxidation activity

Excessive alcohol intake can cause an imbalance in the generation and elimination of free radicals and lead to the production of a large number of free radicals, resulting in lipid peroxidation and decreased antioxidant capacity, thus resulting in hepatocyte damage.[2] Therefore, the antioxidant activity of drugs plays an essential role in liver protection. Fig. 6 shows the scavenging effects of TP, CS-NAC/SA, and CS-NAC/SA/TP on $\cdot$DPPH, $O_2^{\cdot-}$, and $\cdot$OH. The free radical scavenging activity of antioxidant substances is evaluated by the half-maximal inhibitory concentration (IC_{50}). The smaller the IC_{50} value is, the more vital antioxidant ability is.[32] As shown in Fig. 6, single TP and CS-NAC/SA had free radical scavenging activity, and with the increase of sample concentration, the activity of scavenging three free radicals increased. Compared with TP and CS-NAC/SA, CS-NAC/SA/TP showed the most vital antioxidant activity, with IC_{50}s of 2.20 mg mL^{-1}, 2.15 mg mL^{-1}, and 1.26 mg mL^{-1} for $\cdot$DPPH, $O_2^{\cdot-}$, and $\cdot$OH, respectively. Studies have shown that protein hydrolysates and peptides from marine sources have *in vitro* antioxidant activities, including free radical scavenging and lipid peroxidation inhibition.[33] Besides, CS and its derivatives have been proved to be good antioxidants. In particular, the antioxidative and radical scavenging activity of chitosan can be greatly improved by thiolation, which was due to the ability of thiols to form disulfides.[34] They can scavenge excess free radicals in the body, increase antioxidant enzyme activity, and inhibit lipid peroxidation, thus enhancing the antioxidant capacity of the human body.[35] The results suggested that the synergy between CS-NAC and TP underlay the vigorous antioxidant activity of CS-NAC/SA/TP.

3.7 Effects of hydrogel on acute alcoholic liver injury in mice

3.7.1 Effect of hydrogel on the liver index in mice. The liver index can reflect the degree of liver injury, and the results of ethanol-induced acute hepatic injury in mice are shown in Fig. 7. Compared with the normal group, the model group had significantly increased liver index ($p < 0.01$), indicating that acute alcohol consumption significantly increased the liver index. Compared with the model group, the positive and TP groups significantly decreased in the liver index ($p < 0.05$), and
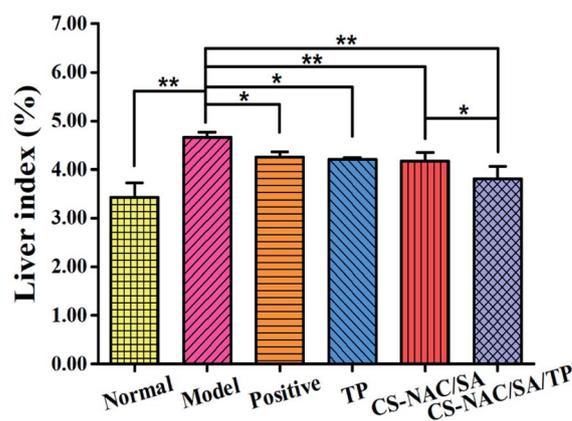

Fig. 7 The liver index of mice ($\bar{x} \pm$ SD, $n = 8$).

CS-NAC/SA and CS-NAC/SA/TP highly significantly decreased ($p < 0.01$). In particular, CS-NAC/SA/TP had a better performance of the liver index (3.81 ± 0.25, $p < 0.05$) compared with CS-NAC/SA. These indicated that CS-NAC/SA/TP could effectively reduce alcoholic liver injury in mice.

3.7.2 Effect of hydrogel on serum AST and ALT contents in mice. AST and ALT are essential indicators of liver injury. Under normal conditions, ALT mainly exists in the cytoplasm of hepatocytes, and AST primarily exists in the cytoplasm and mitochondria. When liver cells are damaged, ALT and AST are released into the serum.[36] Therefore, serum contents of ALT and AST can reflect the degree of hepatocyte injury. The contents of AST and ALT in the serum of mice are shown in Fig. 8. Compared with the normal group, AST and ALT contents in the model group were significantly increased ($p < 0.01$), indicating that excessive alcohol metabolism resulted in enhanced cell membrane permeability and led to the high contents of AST and ALT in the serum. Compared with the model group, AST and ALT contents of TP, CS-NAC/SA, and CS-NAC/SA/TP groups decreased significantly ($p < 0.01$). Notably, compared with CS-NAC/SA, CS-NAC/SA/TP showed the significance in ALT ($p < 0.05$) and high significance in AST ($p < 0.01$), and it almost normalized the serum values of AST and ALT in mice with alcoholic liver injury, which showed that the introduction of TP exerted a combined effect on hepatocyte protection. Taken the above, it demonstrated that CS-NAC/SA/TP had specific protective and reparative effects against alcoholic liver injury.

3.7.3 Effect of hydrogel on ADH and ALDH activities in mouse liver tissue. ADH and ALDH are the main alcohol metabolic enzymes that metabolize about 90% of alcohol in the body. ADH catalyzes the conversion of alcohol into acetaldehyde. Then ALDH catalyzes the conversion of acetaldehyde into acetic acid, which enters the tricarboxylic acid cycle system and is metabolized into water and carbon dioxide.[37] *In vivo*, ADH and ALDH activities can reflect the alcohol-metabolizing ability of hepatocytes. The results of ADH and ALDH activities in mouse liver tissue are shown in Fig. 9. Compared with the normal group, ADH and ALDH activities were significantly increased in the model group ($p < 0.01$), indicating that the liver
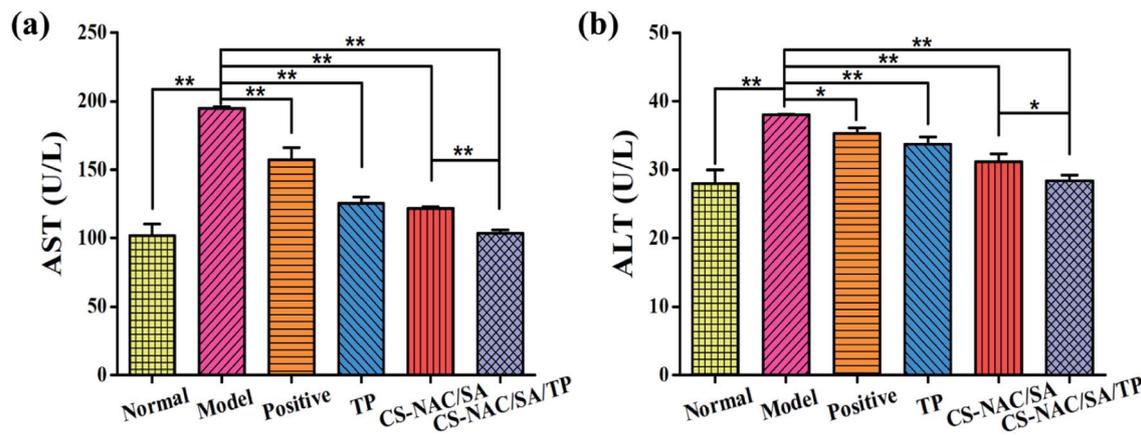
Fig. 8 The contents of (a) AST and (b) ALT in the serum of mice ($\bar{x} \pm$ SD, $n = 8$).
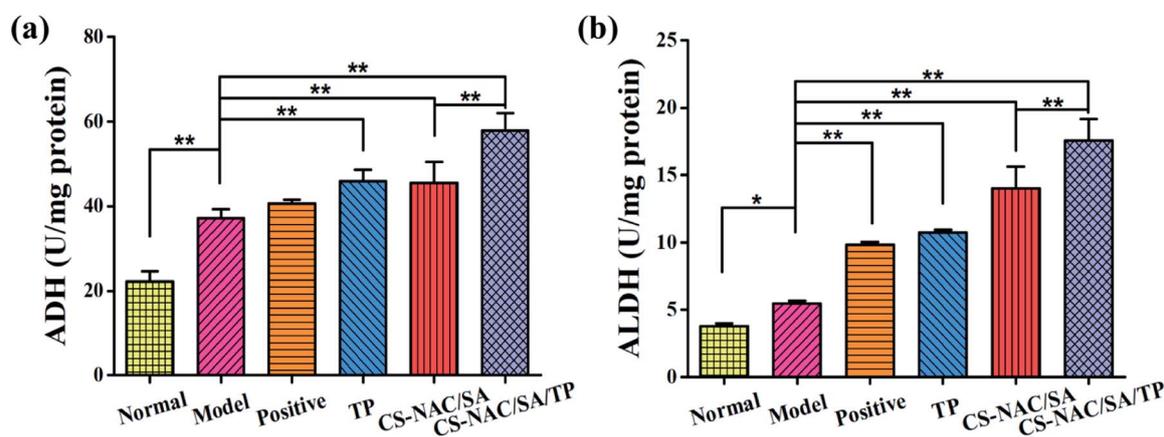

Fig. 9 The activities of (a) ADH and (b) ALDH in mouse liver tissue ($\bar{x} \pm$ SD, $n = 8$).

had a normal metabolic function after the administration of alcohol. Compared with the model group, only ALDH activity significantly increased in the positive group ($p < 0.01$). In contrast, the activities of ADH and ALDH increased significantly in the TP, CS-NAC/SA, and CS-NAC/SA/TP groups ($p < 0.01$), showing that all the selected samples had significantly improved the activities of ADH and ALDH. Especially, CS-NAC/SA/TP had the best performance in improving the activities of ADH and ALDH (ADH 57.83 U per mg per protein; and ALDH 17.58 U per Mg per protein). It was suggested that CS-NAC/SA/TP could increase the activities of ADH and ALDH in liver tissue to metabolize excessive ethanol, thus exerting a protective effect on the liver.

3.7.4 Hematoxylin and eosin (HE) staining. HE staining was performed to observe the degree of liver tissue injury, and the results are shown in Fig. 10. In the normal group, the hepatic lobules were complete, hepatic cords were arranged radially along the central vein, and hepatic sinusoids were clear (Fig. 10(A)). From Fig. 10(B), the hepatic lobules in the model group were disordered and incomplete. Hepatic cord arrangement was disordered, and punctate necrosis and inflammatory cell infiltration could be seen, indicating that gastric alcohol led to severe liver injury in mice. Liver cells in the TP (Fig. 10(D))

and CS-NAC/SA groups (Fig. 10(E)) tended to be arranged in order, but there were also a few inflammatory cells and punctate necrotic cells. In contrast, hepatocytes in the CS-NAC/SA/TP group were orderly arranged, and the hepatic sinusoids were normal (Fig. 10(F)). These results demonstrated that CS-NAC/SA/TP could effectively protect the liver from severe alcohol damage and repair alcohol-induced liver cell injury.

3.8 Effects of hydrogel on chronic alcoholic brain injury in mice

3.8.1 Effect of hydrogel on brain index. The results of mouse brain index are shown in Fig. 11. Compared with the normal group, the values of brain index in the model group were significantly increased ($p < 0.01$), possibly due to brain edema caused by continuous excessive drinking. Compared with the model, TP, CS-NAC/SA, and CS-NAC/SA/TP reduced brain index significantly ($p < 0.01$). Furthermore, among them, CS-NAC/SA/TP had the lowest brain index (1.34 ± 0.02, $p < 0.01$), which was significantly different from CS-NAC/SA ($p < 0.05$). It was suggested that CS-NAC/SA/TP had a strong protective effect against alcoholic brain injury.

3.8.2 Morris water maze. Long-term excessive drinking can significantly change brain structure, physiology, and function.[38]
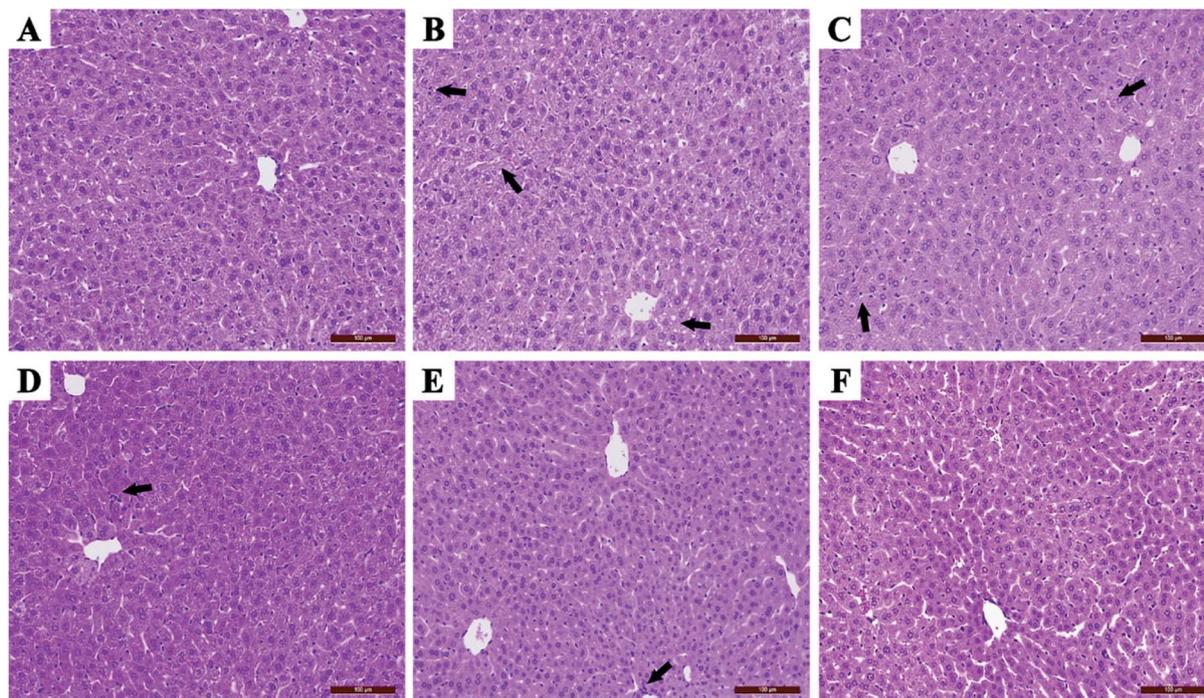
Fig. 10 HE staining (×200) (A) normal, (B) model, (C) positive, (D) TP, (E) CS-NAC/SA, and (F) CS-NAC/SA/TP ($\bar{x} \pm$ SD, $n = 8$). Arrows indicate inflammatory infiltration.

Morris water maze is a recognized method for evaluating the declarative memory function of mice, including location navigation and spatial search. The escape latency during the location navigation experiment represents the ability to acquire memory. And the target quadrant residence time and platform crossing times of the spatial search experiment reflect the memory retention ability.[39] Therefore, Morris water maze was used to determine the degree of brain damage caused by long-term excessive drinking in mice.

The location navigation results are shown in Fig. 12. Compared with the normal group, the escape latency of the model group was prolonged with a significant difference ($p < 0.05$) in the first 3 days and a highly significant difference ($p < 0.01$) after the 4th day, indicating that continuous excessive alcohol intake negatively

affected memory acquisition. Compared with the model group, the escape latency of TP was significantly shortened on the first day ($p < 0.01$), but there was no significant difference after the 4th day, which may result from the decreased TP activity following long-term alcohol consumption. As for CS-NAC/SA and CS-NAC/SA/TP, all the escape latency in 5 days was shortened, especially for CS-NAC/SA/TP with a highly significant difference ($p < 0.01$). The results displayed that CS-NAC/SA/TP exerted a combined effect for protecting and improving the memory acquisition function of mice induced by alcohol.

The spatial search results are shown in Fig. 13. Time in the target quadrant and crossing frequency of the normal group were 16.17 ± 2.58 s and 3.50 ± 0.41, respectively. Compared
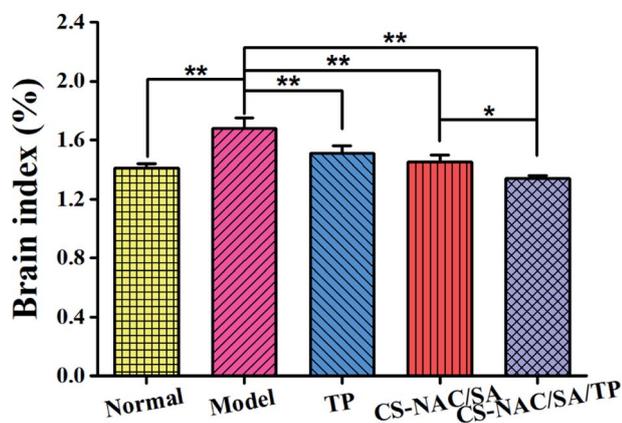

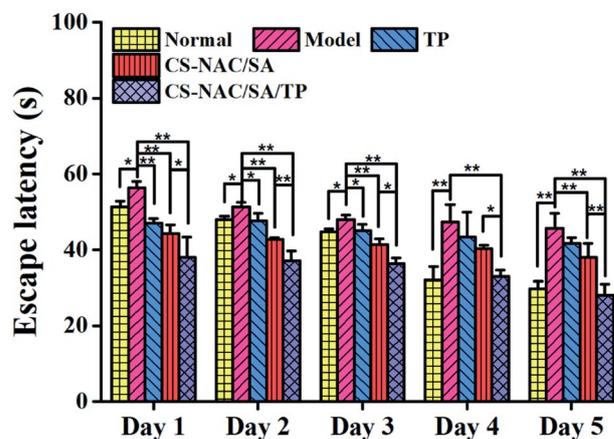**Fig. 11** The brain index of mice ($\bar{x} \pm$ SD, $n = 5$).

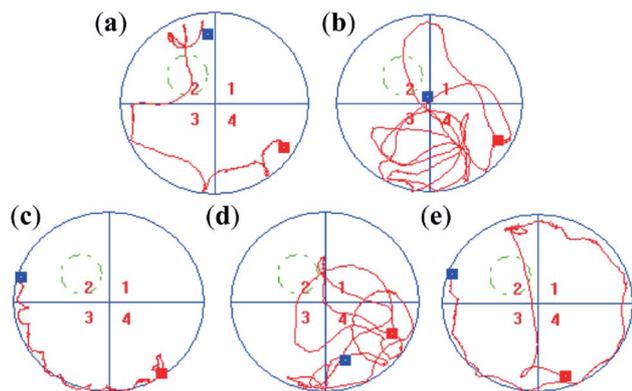**Fig. 12** Mouse Morris location navigation ($\bar{x} \pm$ SD, $n = 5$).

Fig. 13 Representative images of mouse swimming routes after platform removal (a) normal, (b) model, (c) TP, (d) CS-NAC/SA, (e) CS-NAC/SA/TP ($\bar{x} \pm$ SD, $n = 5$).

with the normal group, the model group stayed in the target quadrant (5.83 ± 1.57 s) and crossed the platform (0.71 ± 0.01) significantly less ($p < 0.01$). The movement route was irregular, which indicated that continuous excessive alcohol intake weakened mouse memory ability. In contrast, time in the target quadrant of the mice in TP, CS-NAC/SA, and CS-NAC/SA/TP groups were 8.00 ± 0.76 s, 10.00 ± 1.59 s and 12.00 ± 2.30 s, respectively. And the crossing platform frequency of the mice in TP, CS-NAC/SA, and CS-NAC/SA/TP groups were 1.27 ± 0.24, 1.50 ± 0.29, and 3.00 ± 0.00, respectively. Compared with the model group, the mice in TP, CS-NAC/SA, and CS-NAC/SA/TP groups had longer residence time in the target quadrant and more crossing platform frequency, especially CS-NAC/SA/TP group with a highly significant difference ($p < 0.01$). From the movement routes, it could be seen that the purpose of the mouse in the CS-NAC/SA/TP group search the platform was clear, similar to the normal group. These showed that CS-NAC/SA/TP had a substantial improvement effect on the memory ability in alcohol-injured mice.

4 Conclusions

Using sulfhydryl functionalized chitosan (CS-NAC) and SA as the matrix materials, and introducing TP with antioxidant activity, a gastric acid-response hydrogel was obtained with optimization of RSM based on the results of the single-factor tests. It showed excellent swelling ratio (2350%), good ethanol adsorption (56.23%), and strong antioxidant activities. *In vivo* experiments revealed that CS-NAC/SA/TP had protective effects against alcohol-induced liver and brain injuries in mice by reducing the contents of serum ALT and AST and enhancing liver activities of ADH and ALDH. In summary, CS-NAC/SA/TP had promising applications in the prevention of alcohol-induced liver and brain injuries.

Ethical statement

All animal procedures were performed in accordance with the Guidelines for Care and Use of Laboratory Animals of

Guangdong Ocean University and experiments were approved by the Animal Ethics Committee of Guangdong Ocean University (SYXK-20180147).

Conflicts of interest

There are no conflicts to declare.

Acknowledgements

References

1 N. Hosseini, J. Shor and G. Szabo, *Alcohol Alcohol.*, 2019, **54**, 408–416.

2 A. Louvet and P. Mathurin, *Nat. Rev. Gastroenterol. Hepatol.*, 2015, **12**, 231–242.

3 N. M. Zahr, K. L. Kaufman and C. G. Harper, *Nat. Rev. Neurol.*, 2011, 7, 284–294.

4 P. P. Lowe, C. Morel, A. Ambade, A. Iracheta-Vellve, E. Kwiatkowski, A. Satishchandran, I. Furi, Y. Cho, B. Gyongyosi, D. Catalano, E. Lefebvre, L. Fischer, S. Seyedkazemi, D. P. Schafer and G. Szabo, *J. Neuroinflammation*, 2020, **17**, 296.

5 Y. Tu, S. Zhu, J. Wang, E. Burstein and D. Jia, *Phytother. Res.*, 2019, **33**, 2192–2212.

6 Z. Zhang, H. Zhou, L. Bai, Y. Lv, H. Yi, L. Zhang and R. Li, *J. Funct. Foods*, 2019, **59**, 234–241.

7 K. Ohashi, M. Pimienta and E. Seki, *Liver Res.*, 2018, **2**, 161–172.

8 T. S. Sehrawat, M. Liu and V. H. Shah, *Lancet. Gastroenterol. Hepatol.*, 2020, **5**, 494–506.

9 S. H. Aswathy, U. Narendrakumar and I. Manjubala, *Heliyon*, 2020, **6**, e03719.

10 S. Sharma and S. Tiwari, *Int. J. Biol. Macromol.*, 2020, **162**, 737–747.

11 K. Varaprasad, G. M. Raghavendra, T. Jayaramudu, M. M. Yallapu and R. Sadiku, *Mater. Sci. Eng., C*, 2017, **79**, 958–971.

12 B. Qu and Y. Luo, *Int. J. Biol. Macromol.*, 2020, **152**, 437–448.

13 M. Vakili, M. Rafatullah, B. Salamatinia, A. Z. Abdullah, M. H. Ibrahim, K. B. Tan, Z. Gholami and P. Amouzgar, *Carbohydr. Polym.*, 2014, **113**, 115–130.

14 K. Varaprasad, T. Jayaramudu, V. Kanikireddy, C. Toro and E. R. Sadiku, *Carbohydr. Polym.*, 2020, **236**, 116025.

15 M. Zhang and X. Zhao, *Int. J. Biol. Macromol.*, 2020, **162**, 1414–1428.

16 M. Ahmed, A. K. Verma and R. Patel, *Sustainable Chem. Pharm.*, 2020, **18**, 100315.

17 Z. Hu, P. Yang, C. Zhou, S. Li and P. Hong, *Mar. Drugs*, 2017, **15**, 102.

18 A. Jakubczyk, M. Karas, K. Rybczynska-Tkaczyk, E. Zielinska and D. Zielinski, *Foods*, 2020, **9**, 846.

19 R. M. Raftery, B. Woods, A. L. P. Marques, J. Moreira-Silva, T. H. Silva, S. A. Cryan, R. L. Reis and F. J. O'Brien, *Acta Biomater.*, 2016, **43**, 160–169.

20 X. Wang, C. Zheng, Z. Wu, D. Teng, X. Zhang, Z. Wang and C. Li, *J. Biomed. Mater. Res., Part B*, 2009, **88**, 150–161.

21 X. Hu, Y. Wang, L. Zhang and M. Xu, *Carbohydr. Polym.*, 2020, **234**, 115920.

22 G. Porter, D. Schwass, G. Tompkins, S. Bobbala, N. Medlicott and C. Meledandri, *Carbohydr. Polym.*, 2021, **251**, 117017.

23 E. Kim, M. H. Kim, J. H. Song, C. Kang and W. H. Park, *Int. J. Biol. Macromol.*, 2020, **154**, 989–998.

24 S. Potiwiput, H. Tan, G. Yuan, S. Li, T. Zhou, J. Li, Y. Jia, D. Xiong, X. Hu, Z. Ling and Y. Chen, *Mater. Chem. Phys.*, 2020, **241**, 122354.

25 D. Zhang, Z. Hu, S. Lu, S. Li, Z. Yang and P. Li, *IOP Conf. Ser.: Mater. Sci. Eng.*, 2019, **629**, 012038.

26 S. Mallakpour and E. Khadem, *Int. J. Biol. Macromol.*, 2018, **114**, 149–160.

27 N. D. Al-Jbour, M. D. Beg, J. Gimbun and A. K. M. M. Alam, *Curr. Drug Delivery*, 2019, **16**, 272–294.

28 Y. Guo, F. Zhao, X. Zhou, Z. Chen and G. Yu, *Nano Lett.*, 2019, **19**, 2530–2536.

29 J. G. Fernandez and D. E. Ingber, *Adv. Mater.*, 2012, **24**(4), 480–484.

30 G. Yang, M. Wu, H. Yi and J. Wang, *Mater. Sci. Eng., C*, 2016, **59**, 278–285.

31 C. Federer, M. Kurpiers and A. Bernkop-Schnurch, *Biomacromolecules*, 2021, **22**, 24–56.

32 Y. Qin, J. Xie, B. Xue, X. Li, J. Gan, T. Zhu and T. Sun, *Food Hydrocolloids*, 2021, **112**, 106284.

33 L. Amigo and B. Hernandez-Ledesma, *Molecules*, 2020, **25**, 4479.

34 K. Chauhan, R. Sharma, R. Dharela, G. S. Chauhan and R. K. Singhal, *RSC Adv.*, 2016, **6**, 75453–75464.

35 W. Wang, C. Xue and X. Mao, *Int. J. Biol. Macromol.*, 2020, **164**, 4532–4546.

36 X. Jiang, Y. Zhou, Y. Zhang, D. Tian, S. Jiang and Y. Tang, *Process Biochem.*, 2020, **92**, 303–312.

37 J. Zheng, X. Tian, W. Zhang, P. Zheng, F. Huang, G. Ding and Z. Yang, *Mar. Drugs*, 2019, **17**, 552.

38 A. Jacob and P. Wang, *Front. Neurosci.*, 2020, **14**, 102.

39 M. D. Whiting and O. N. Kokiko-Cochran, *Methods Mol. Biol.*, 2016, **1462**, 553–571.